All-dielectric planar chiral metasurface with gradient geometric phase

ZHIJIE MA,[1,2,3,4] YI LI,[3] YANG LI,[2] YANDONG GONG,[4,5] STEFAN A. MAIER,[3,6] AND MINGHUI HONG[2,*]

[1]NUS Graduate School for Integrative Sciences & Engineering (NGS), National University of Singapore, Singapore, 117456, Singapore
[2]Department of Electrical and Computer Engineering, National University of Singapore, 117576, Singapore
[3]Department of Physics, Imperial College London, London SW7 2AZ, UK
[4]Institute for Infocomm Research, A*STAR, 138632, Singapore
[5]Institute of Lightwave Technology, Beijing Jiaotong University, Beijing 100044, China
[6]Faculty of Physics, Ludwig-Maximilians-Universitat Munchen, 80799 Munchen, Germany
[*]elehmh@nus.edu.sg

Abstract: Planar optical chirality of a metasurface measures its differential response between left and right circularly polarized (CP) lights and governs the asymmetric transmission of CP lights. In 2D ultra-thin plasmonic structures the circular dichroism is limited to 25% in theory and it requires high absorption loss. Here we propose and numerically demonstrate a planar chiral all-dielectric metasurface that exhibits giant circular dichroism and transmission asymmetry over 0.8 for circularly polarized lights with negligible loss, without bringing in bianisotropy or violating reciprocity. The metasurface consists of arrays of high refractive index germanium Z-shape resonators that break the in-plane mirror symmetry and induce cross-polarization conversion. Furthermore, at the transmission peak of one handedness, the transmitted light is efficiently converted into the opposite circular polarization state, with a designated geometric phase depending on the orientation angle of the optical element. In this way, the optical component sets before and after the metasurface to filter the light of certain circular polarization states are not needed and the metasurface can function under any linear polarization, in contrast to the conventional setup for geometry phase based metasurfaces. Anomalous transmission and two-dimensional holography based on the geometric phase chiral metasurface are numerically demonstrate as proofs of concept.

References and links

1. Y. Cui, L. Kang, S. Lan, S. Rodrigues, and W. Cai, "Giant chiral optical response from a twisted-arc metamaterial," Nano Lett. **14**, 1021–1025 (2014).
2. L. D. Barron, *Molecular Light Scattering and Optical Activity* (Cambridge University, 2009).
3. V. K. Valev, J. J. Baumberg, C. Sibilia, and T. Verbiest, "Chirality and chiroptical effects in plasmonic nanostructures: Fundamentals, recent progress, and outlook," Adv. Mat. **25**, 2517–2534 (2013).
4. J. K. Gansel, M. Thiel, M. S. Rill, M. Decker, K. Bade, V. Saile, G. von Freymann, S. Linden, and M. Wegener, "Gold Helix Photonic Metamaterial as Broadband Circular Polarizer," Science **325**, 1513–1515 (2009).
5. R. Ji, S. W. Wang, X. Liu, H. Guo, and W. Lu, "Hybrid Helix Metamaterials for Giant and Ultrawide Circular Dichroism," ACS Photonics **3**, 2368–2374 (2016).
6. E. Plum, V. A. Fedotov, A. S. Schwanecke, N. I. Zheludev, and Y. Chen, "Giant optical gyrotropy due to electromagnetic coupling," App. Phys. Lett. **90**, 12–15 (2007).
7. M. Decker, R. Zhao, C. M. Soukoulis, S. Linden, and M. Wegener, "Twisted split-ring-resonator photonic metamaterial with huge optical activity," Opt. Lett. **35**, 1593 (2010).
8. N. Liu, H. Liu, S. Zhu, and H. Giessen, "Stereometamaterials," Nat. Photonics **3**, 157–162 (2009).
9. M. Hentschel, L. Wu, M. Sch?ferling, P. Bai, E. P. Li, and H. Giessen, "Optical properties of chiral three-dimensional plasmonic oligomers at the onset of charge-transfer plasmons," ACS Nano **6**, 10355–10365 (2012).
10. Y. Zhao, M. A. Belkin, and A. Al?, "Twisted optical metamaterials for planarized ultrathin broadband circular polarizers," Nat. Commun. **3**, 870 (2012).

11. R. Zhao, L. Zhang, J. Zhou, T. Koschny, and C. M. Soukoulis, "Conjugated gammadion chiral metamaterial with uniaxial optical activity and negative refractive index," Phys. Rev. B **83**, 4–7 (2011).
12. Z. Wang, F. Cheng, T. Winsor, and Y. Liu, "Optical chiral metamaterials: a review of the fundamentals, fabrication methods and applications," Nanotechnology **27**, 412001 (2016).
13. V. A. Fedotov, P. L. Mladyonov, S. L. Prosvirnin, A. V. Rogacheva, Y. Chen, and N. I. Zheludev, "Asymmetric propagation of electromagnetic waves through a planar chiral structure," Phys. Rev. Lett. **97**, 1–4 (2006).
14. V. A. Fedotov, A. S. Schwanecke, N. I. Zheludev, V. V. Khardikov, and S. L. Prosvirnin, "Asymmetric transmission of light and enantiomerically sensitive plasmon resonance in planar chiral nanostructures," Nano Lett. 7, 1996−1999 (2007).
15. A. S. Schwanecke, V. A. Fedotov, V. V. Khardikov, S. L. Prosvirnin, Y. Chen, and N. I. Zheludev, "Nanostructured Metal Film with Asymmetric Optical Transmission 2008," Nano Lett. **8**, 2940–2943 (2008).
16. A. B. Khanikaev, N. Arju, Z. Fan, D. Purtseladze, F. Lu, J. Lee, P. Sarriugarte, M. Schnell, R. Hillenbrand, M. A. Belkin, and G. Shvets, "Experimental demonstration of the microscopic origin of circular dichroism in two-dimensional metamaterials," Nat. Commun. **7**, 12045 (2016).
17. C. Pfeiffer, C. Zhang, V. Ray, L. J. Guo, and A. Grbic, "High performance bianisotropic metasurfaces: Asymmetric transmission of light," Phys. Rev. Lett. **113**, 1–5 (2014).
18. J. M. Geffrin, B. Garc?a-C?mara, R. G?mez-Medina, P. Albella, L. S. Froufe-P?rez, C. Eyraud, A. Litman, R. Vaillon, F. Gonzalez, M. Nieto-Vesperinas, J. J. S?enz, and F. Moreno, "Magnetic and electric coherence in forward- and back-scattered electromagnetic waves by a single dielectric subwavelength sphere.," Nat. Commun. **3**, 1171 (2012).
19. Z. Ma, S. M. Hanham, P. Albella, B. Ng, H. T. Lu, Y. Gong, S. A. Maier, and M. Hong, "Terahertz All-Dielectric Magnetic Mirror Metasurfaces," ACS Photonics **3**, 1010−1018 (2016).
20. C. Menzel, C. Rockstuhl, and F. Lederer, "Advanced Jones calculus for the classification of periodic metamaterials," Phys. Rev. A **82**, 1–9 (2010).
21. C. Menzel, C. Helgert, C. Rockstuhl, E. B. Kley, A. Tunnermann, T. Pertsch, and F. Lederer, "Asymmetric transmission of linearly polarized light at optical metamaterials," Phys. Rev. Lett. **104**, 1–4 (2010).
22. J. Kong, *Electromagnetic Wave Theory* (John Wiley & Sons, 2002).
23. E. D. Palik, *Handbook of Optical Constants of Solids* (Academic, 1985).
24. D. Jalas, A. Petrov, M. Eich, W. Freude, S. Fan, Z. Yu, R. Baets, M. Popovic, A. Melloni, J. D. Joannopoulos, M. Vanwolleghem, C. R. Doerr, and H. Renner, "What is – and what is not – an optical isolator," Nat. Photonics **7**, 579–582 (2013).
25. A. Arbabi and A. Faraon, "Fundamental limits of ultrathin metasurfaces," Sci. Rep. **7**, 43722 (2014).
26. X. Ding, F. Monticone, K. Zhang, L. Zhang, D. Gao, S. Nawaz Burokur, A. De Lustrac, Q. Wu, C. W. Qiu, and A. Al?, "Ultrathin pancharatnam-berry metasurface with maximal cross-polarization efficiency," Adv. Mat. **27**, 1195–1200 (2015).
27. M. Kerker, D. S. Wang, and C. L. Giles, "Electromagnetic scattering by magnetic spheres," Opt Express **73**, 765–767 (1983).
28. C. Wu, N. Arju, G. Kelp, J. A. Fan, J. Dominguez, E. Gonzales, E. Tutuc, I. Brener, and G. Shvets, "Spectrally selective chiral silicon metasurfaces based on infrared Fano resonances," Nat. Commun. **5**, 3892 (2014).
29. J. Hu, X. Zhao, Y. Lin, A. Zhu, X. Zhu, P. Guo, B. Cao, and C. Wang, "All-dielectric metasurface circular dichroism waveplate," Sci. Rep. **7**, 41893 (2017).
30. R. Alaee, M. Albooyeh, M. Yazdi, N. Komjani, C. Simovski, F. Lederer, and C. Rockstuhl, "Magnetoelectric coupling in nonidentical plasmonic nanoparticles: Theory and applications," Phys. Rev. B **91**, 115119 (2015).
31. M. Odit, P. Kapitanova, P. Belov, R. Alaee, C. Rockstuhl, and Y. S. Kivshar, "Experimental realisation of all-dielectric bianisotropic metasurfaces," App. Phys. Lett. **108**, 221903 (2016).
32. C. E. Kriegler, M. S. Rill, S. Linden, and M. Wegener, "Bianisotropic photonic metamaterials," IEEE J. Sel. Topics Quantum Electron. **16**, 367–375 (2010).
33. A. V. Kildishev, J. D. Borneman, X. Ni, V. M. Shalaev, and V. P. Drachev, "Bianisotropic effective parameters of optical metamagnetics and negative-index materials," Proc. IEEE **99**, 1691–1700 (2011).
34. X. Chen, B. I. Wu, J. A. Kong, and T. M. Grzegorczyk, "Retrieval of the effective constitutive parameters of bianisotropic metamaterials," Phys. Rev. E, **71**, 046610 (2005). .
35. X. Ma, M. Pu, X. Li, C. Huang, Y. Wang, W. Pan, B. Zhao, J. Cui, C. Wang, Z. Zhao, and X. Luo, "A planar chiral meta-surface for optical vortex generation and focusing," Sci. Rep. **5**, 10365 (2015).
36. Y. W. Huang, W. T. Chen, W. Y. Tsai, P. C. Wu, C. M. Wang, G. Sun, and D. P. Tsai, "Aluminum plasmonic multicolor meta-Hologram," Nano Lett. **15**, 3122–3127 (2015).
37. A. Arbabi, Y. Horie, M. Bagheri, and A. Faraon, "Dielectric Metasurfaces for Complete Control of Phase and Polarization with Subwavelength Spatial Resolution and High Transmission," Nat. Nanotechnology **10**, 937–943 (2014).
38. M. Decker, I. Staude, M. Falkner, J. Dominguez, D. N. Neshev, I. Brener, T. Pertsch, and Y. S. Kivshar, "High-Efficiency Dielectric Huygens' Surfaces," Adv. Opt. Mat. **3**, 813–820 (2015).
39. Z. Bomzon, G. Biener, V. Kleiner, and E. Hasman, "Space-variant Pancharatnam-Berry phase optical elements with computer-generated subwavelength gratings," Opt. Lett. **27**, 1141 (2002).
40. L. Huang, X. Chen, H. M?hlenbernd, H. Zhang, S. Chen, B. Bai, Q. Tan, G. Jin, K.-W. Cheah, C.-W. Qiu, J. Li, T. Zentgraf, and S. Zhang, "Three-dimensional optical holography using a plasmonic metasurface.," Nat. Commun. **4**,

2808 (2013).
41. G. Li, M. Kang, S. Chen, S. Zhang, E. Y. B. Pun, K. W. Cheah, and J. Li, "Spin-enabled plasmonic metasurfaces for manipulating orbital angular momentum of light," Nano Lett. **13**, 4148–4151 (2013).
42. L. Jing, Z. Wang, R. Maturi, B. Zheng, H. Wang, Y. Yang, L. Shen, R. Hao, W. Yin, E. Li, and H. Chen, "Gradient Chiral Metamirrors for Spin-Selective Anomalous Reflection," Laser Photon. Rev. **11**, 1700115 (2017).
43. I. V Il'ina, T. Y. Cherezova, and A. V Kudryashov, "Gerchberg-Saxton algorithm: experimental realisation and modification for the problem of formation of multimode laser beams," Quantum Electron. **39**, 521–527 (2009).
44. T. Liu, J. Tan, J. Liu, and H. Wang, "Vectorial design of super-oscillatory lens," Opt. Express **21**, 15090 (2013).

1. Introduction

Left and right circular polarizations are spin eigenstates of a photon. As light propagates, the instant electric field vector traces out a helical trajectory, which is intrinsically chiral, meaning that its mirror image 'cannot be brought to coincide with itself' (Lord Kelvin). Naturally, the two circularly polarized (CP) lights interact differently with three dimensional chiral structures, which exists widely in certain crystals and ubiquitously in the organic world, including the most common amino acids and sugar molecules [1]. In chiral molecules (also called 'enantiomers'), both the real and imaginary parts (extinction coefficient) of the refractive index vary for left and right circularly polarized light, giving rise to chiroptical effects such as optical activity (circular birefringence) and circular dichroism (CD), respectively [2]. Optical activity and circular dichroism measurements with chiral materials have been applied in analytical chemistry, crystallography, and pharmaceutical industries to determine the structure handedness of the molecules and the concentration [3]. However, due to the large scale mismatch between the wavelength of CP lights and the molecule sizes, the interaction is generally weak and a long optical path is often required to show noticeable differences for left circularly polarized (LCP) and right circularly polarized (RCP) lights.

To overcome the issue of small chirality response in natural materials, metamaterials have been introduced to boost the chiroptical performances in orders of magnitude. Three dimensional chiral metamaterials such as metallic helical stereostructures have been fabricated to function as highly efficient broadband circular polarizers [4, 5], with greatly reduced thickness comparing to conventional circular polarizers made by the combination of linear polarizer and quarter waveplate (QWP). Twisted multi-layer cascaded structures are also commonly used to achieve giant optical chirality [6–11]. However, most of these metal-based three dimensional chiral metamaterials demands sophisticated fabrication processes and exhibit unavoidable absorption losses [12]. Planar chiral structures with broken in-plane mirror symmetry have been explored to avoid the fabrication complexity. The first single-layer planar metamaterial that shows significant difference for LCP and RCP lights was realized by fish-scale plasmonic structure, with enantiomerically selective plasmon resonance modes [13–15]. However, in the fish-scale and other ultra-thin non-magnetic plasmonic structures [16], only electric currents are excited on the plane, without magnetic response, in this case, the scattered fields are symmetric in the forward and backward directions. In consequence, the asymmetric transmission is theoretically limited to 25% and it can only be realized when the absorption loss reaches its theoretical maximum of 50% [17].

Recently, dielectric metamaterials have attracted great interest for their low absorption loss, high refractive index, great field enhancement inside the resonator, and the capability of exciting higher order Mie resonance modes, offering higher efficiency and more degrees of freedom for light manipulation. However, up until now, there have only been few studies on the optical chirality of dielectric metasurfaces [28, 29] and a dielectric chiral metasurface with gradient phase has not been demonstrated.

In this article, we propose a low-loss planar-chiral all-dielectric metasurface that exhibits giant circular dichroism and asymmetric transmission value close to unity for circularly polarized lights, free from the 25% limit and the loss requirement. The broken in-plane mirror symmetry of the metasurface leads to linear cross-polarization generation, and the finite thickness of the
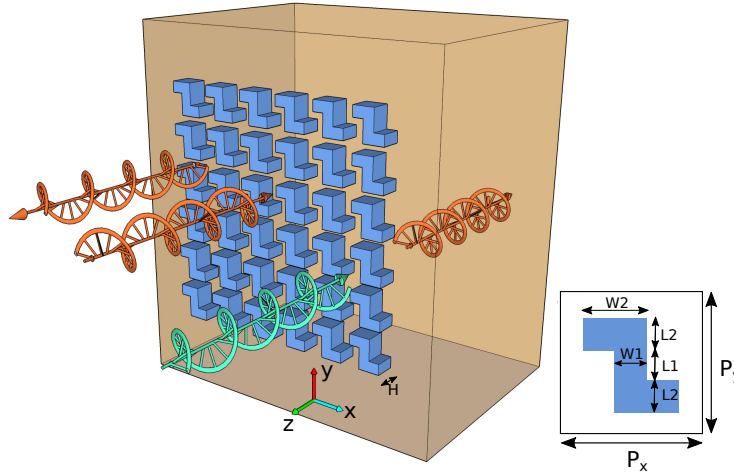
Fig. 1. Illustration of the chiral metasurface with giant transmission difference to left- and right-circularly polarized lights. The RCP and LCP lights are represented with blue and brown colors, respectively. The structure consists of germanium Z-shape resonators on SiO_2 substrate, and the inset shows the geometrical parameters W1 = 205 nm, W2 = 410 nm, L1 = 205 nm, L2 = 205 nm, thickness H = 500 nm, and periodicity P_x = P_y = 900 nm.

dielectric metasurface enables the excitation of both the electric and magnetic resonances that break the radiation symmetry in the forward and backward directions [18, 19]. Furthermore, the light transmitted through the metasurface is efficiently converted to the orthogonal circular polarization and a geometric phase can be endowed by simply controlling the orientation angle of the resonator element. The metasurface can effectively operate as an "all-in-one device" equivalent to a cascaded combination of a linear polarizer, a quarter waveplate, a spatial light modulator, followed by another linear polarizer and quarter waveplate. The concept is numerically verified with examples including anomalous transmission and a two-dimensional computer generated hologram with high efficiency of 0.6.

2. Results and discussion

We begin with the generation of transmission circular dichroism. The transmission of light through a given interface in a linear base can be represented by the Jones matrix. When converted to the circular base, the complex transmission coefficients for circular polarizations are related to the linear Jones matrix through:

$$\begin{pmatrix} t_{ll} & t_{lr} \\ t_{rl} & t_{rr} \end{pmatrix} = \frac{1}{2} \begin{pmatrix} t_{xx} + t_{yy} + i(t_{yx} - t_{xy}) & t_{xx} - t_{yy} - i(t_{xy} + t_{yx}) \\ t_{xx} - t_{yy} + i(t_{yx} + t_{xy}) & t_{xx} + t_{yy} - i(t_{xy} - t_{yx}) \end{pmatrix} \tag{1}$$

where the first (second) sub-index stands for polarization state of the transmitted (incident) light, and 'l' and 'r' correspond to left and right handedness, respectively. For planar metasurfaces with no variation in the propagation direction z, this mirror symmetry condition ensures that the transmission coefficient $t_{xy} = t_{yx}$ [20, 21], and the relationship between the transmitted circularly polarized light and the incidence can be simplified as:

$$\begin{pmatrix} E_{tl} \\ E_{tr} \end{pmatrix} = \frac{1}{2} \begin{pmatrix} t_{xx} + t_{yy} & t_{xx} - t_{yy} - 2it_{xy} \\ t_{xx} - t_{yy} + 2it_{xy} & t_{xx} + t_{yy} \end{pmatrix} \begin{pmatrix} E_{il} \\ E_{ir} \end{pmatrix} \tag{2}$$
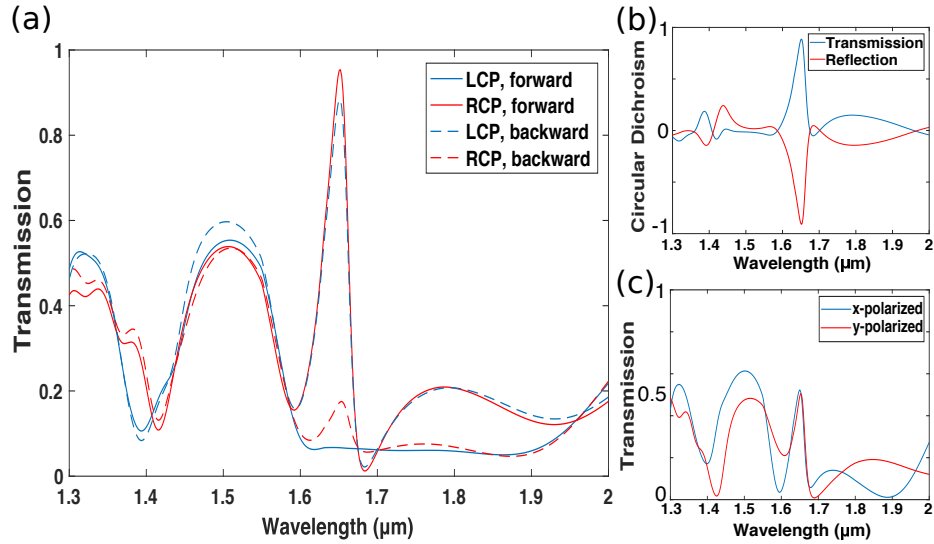
Fig. 2. (a) Transmission spectra for LCP and RCP incidences in forward and backward directions. (b) Transmission and reflection circular dichroisms of the metasurface. (c) Transmission spectra of the metasurface under x and y linear polarization incidences.

As a result, $t_{ll} = t_{rr} = t_{xx} + t_{yy}$, and $T_{LL} = T_{RR}$, where $T_{LL} = |t_{ll}|^2$ and $T_{RR} = |t_{rr}|^2$ are the polarization handedness-preserved transmittance, and they are the same for the two circular polarizations.

However, when $t_{xy} \neq 0$, the transmission circular cross-polarization conversion rate $T_{LR} \neq T_{RL}$, where $T_{LR} = |t_{rl}|^2$ and $T_{RL} = |t_{lr}|^2$. As a consequence, the total transmission for left circularly polarized (LCP) incident light $T_L \equiv T_{LL} + T_{RL}$ can be distinct from that for right circularly polarized (RCP) incidence $T_R \equiv T_{RR} + T_{LR}$. The transmission circular dichroism (CD) is defined as $\Delta T = T_R - T_L$. For any 2D structure with in-plane mirror symmetry, the Jones matrix can be diagonalized so that $t_{xy} = t_{yx} = 0$, no linear cross-polarization conversion can occur, consequently, the CD value must be zero [20]. Therefore, in order to have a nonzero CD, the in-plane mirror symmetry must be broken in 2D metasurfaces.

In planar chiral metasurfaces, here we emphasize a particular situation where $t_{xx} = -t_{yy} = it_{xy} = it_{yx} = 0.5$. In this case, the circular basis transmission matrix becomes $M = \begin{pmatrix} 0 & 1 \\ 0 & 0 \end{pmatrix}$, the power transmission coefficients for circular base are $T_{LL} = T_{RR} = T_{LR} = 0$, and $T_{LR} = 1$. For the LCP incidence, destructive interference in the transmission direction occurs between the scattered lights from the x- and y-polarized components, while for the RCP incidence, they interfere constructively and generate high transmittance, with CD = 1, and the RCP light is totally converted into LCP state. To verify this operating principle, we design a single-layer all-dielectric metasurface that approximates the transmission coefficients requirement. The structure of the metasurface is schematically shown in Fig. 1, with the geometry parameters denoted in the inset figure. The metasurface are composed of periodic arrays of Z-shape germanium resonators (n~4.2), with W1 = 205 nm, W2 = 410 nm, L1 = 205 nm, L2 = 205 nm, and thickness H = 500 nm. To avoid high-order diffractions, the periodicity is set in a sub-wavelength scale, with $P_x = P_y = 900$ nm for x and y directions. Germanium is chosen for its high refractive index and low absorption loss in the infrared regime. For practical realization, the planar chiral elements are supported by a semi-infinite SiO_2 substrate in simulations, with the refractive index set constant
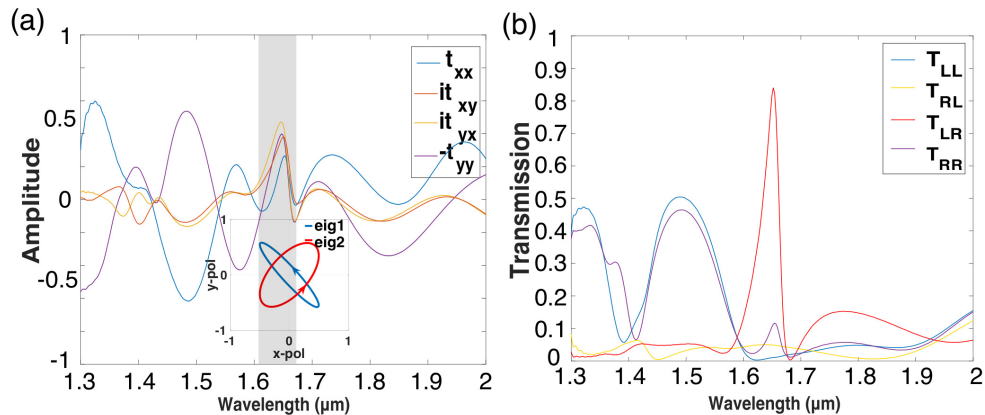
Fig. 3. (a) The transmission coefficients t_{xx}, it_{xy}, it_{yx}, and $-t_{yy}$ of the metasurface. Inset: polarization eigenstates at 1655 nm, showing two co-rotating elliptical polarizations. (b) The co- and cross-polarization transmittance coefficients T_{LL}, T_{RL}, T_{LR}, and T_{RR} of the metasurface.

as 1.45. The optical dielectric functions of Ge and SiO$_2$ were taken from Palik's Handbook [23]. As shown in Fig. 1, circularly polarized lights are normally incident on the chiral metasurface from the air side along the -z-axis, which is defined as the forward direction of propagation, and the z-axis direction is defined as the backward propagation direction for the succeeding discussion.

In Fig. 2(a), the solid lines show the transmission spectra for LCP and RCP lights incident in forward direction of propagation. At 1655 nm, the transmission for RCP reaches 0.95, in contrast, for LCP incidence the transmission is only 0.07, returning a large CD value of 0.88. For a 2D chiral metasurface, the sense of twist is reversed when observed from the opposite direction. The transmission for circularly polarized light of one handedness in the forward direction is equivalent to the transmission for the other polarization handedness propagating in the backward direction. Therefore, planar chirality also demonstrates itself as asymmetric transmission (AT). The power transmissions for LCP and RCP lights in the opposite propagating directions are plotted with dashed lines in Fig. 2(a). For LCP, at $\lambda = 1655$ nm, the transmission asymmetry is as high as 0.8. This seemingly nonreciprocal phenomenon in planar chiral metasurface actually does not violate the Lorentz reciprocity nor the time-reversal symmetry [22], in contrast to the nonreciprocal transmissions in magneto-optical or nonlinear media [24]. It should be noted that the small discrepancy between the transmissions for 'LCP, forward' and 'RCP, backward' is due to the presence of the substrate which slightly breaks the mirror symmetry in the z-direction with the refractive index change. In Fig. 2(b), the CD spectra are plotted for both the transmission and reflection, due to the low absorption loss in germanium above 1.5 μm, the incident light is either transmitted or reflected, leading to the CD for transmission and reflection being approximately opposite to each other. The transmission spectra of the metasurface under linear x and y-polarization are also plotted in Fig. 2(c). As any linear polarization (LP) state can be considered as the superposition of RCP and LCP states, under LP illuminations on the metasurface, at the resonance peak $\lambda = 1655$ nm, the RCP component is transmitted with high efficiency while the LCP component is highly reflected, therefore, the transmission for either x or y-polarized light is close to 0.5.

To examine how well the proposed metasurface approximates the condition for the anomalous

RCP, 1655 nm   LCP, 1655 nm   RCP, 2000 nm
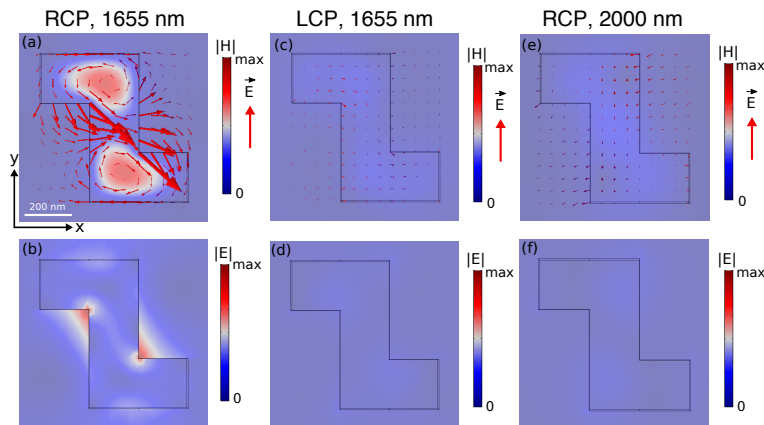
Fig. 4. (a) The magnetic near-field and electric vector, and (b) the electric near-field distributions in the Z-shape resonator under RCP incidence, at λ = 1655 nm. (c, d) The magnetic and electric near-field under LCP incidence, at λ = 1655 nm. (e, f) The magnetic and electric near-field under RCP incidence, at λ = 2000 nm. The subfigures in the same rows are in the same scale.

circular selective transmission in the analysis above, the t_{xx}, it_{yx}, it_{xy}, and $-t_{yy}$ transmission coefficients of the Jones matrix are plotted in Fig. 3(a). The coefficients are dispersive because of the resonance nature of the metasurfaces. It can be observed that t_{xy} is close to t_{yx} over the spectrum, and the values of the four coefficients are close near the resonance in the highlighted area. Based on the transmission matrix, the polarization eigenstates at 1655 nm are calculated. The metasurface has two co-rotating elliptical polarization eigenstates as shown in the inset of Fig. 3(a), which agrees with the predication by symmetry requirement [20]. In Fig. 3(b), the transmitted waves under different circular polarization incidences are decomposed into the LCP and RCP components; the four transmittance coefficients T_{LL}, T_{RL}, T_{LR}, and T_{RR} in circular basis are plotted. At the resonance peak, for the RCP incidence, the cross-polarization conversion rate into LCP is larger than 0.8, as shown by the red solid line T_{LR}. It can be observed that there is still some co-polarized state transmitted as the metasurface is not a perfect realization of the strict conditions in the analysis, but the ratio of T_{LR} over T_{RR} is still kept as high as 8:1. For LCP incidence, in the interested wavelength range, the total transmission is lower than 0.1, and T_{RL} is only around 0.05.

In Fig. 4, the magnetic and electric near-field distributions are plotted for each circular polarization incidence in a z-normal cut plane in the middle of the meta-atom. At 1655 nm, for RCP incidence, we observe two magnetic field enhancement nodes inside the resonator pointing in z-direction, with electric field vector circulating around the magnetic field maximum in each arm, and the electric field is concentrated at the corner outside the resonator. In contrast, the electric and magnetic near-fields under LCP incidence are much weaker and we can hardly observe any field enhancement in Fig. 4(c) and 4(d), suggesting that the resonance modes are circular polarization selective in the chiral metasurface. The field distributions are also plotted for RCP incidence at 2000 nm in Fig. 4(e) and 4(f), which show that at non-resonant frequency, the modes are not excited and the fields enhancement is very insignificant. Due to the complexity of the structure geometry, the meta-atom cannot be readily described by the superposition of point multipoles, further investigations will be needed for a complete multipole analysis and it is out of the scope of this work.

The circular dichroism as high as 0.8 in our planar chiral metasurface significantly surpasses the 25% theoretical limit in single layer plasmonic chiral metasurfaces [16], such as the earliest

fishnet structure [13, 14]. The 25% limit is imposed by the symmetric scattering from an ultra-thin planar structure where only tangential electrical currents are supported [25, 26], and the theoretical limit can only be reached when the metasurface meets the maximum absorption of 50 % [13, 14]. However, Kerker *et al.* demonstrated that highly asymmetric full forward scattering or strong backward scattering of a particle can be achieved by the interference of the electric dipole and magnetic dipole modes of a scatterer [18, 27]. Magnetic dipole and other higher order modes can be excited in our proposed and other dielectric metasurfaces [28, 29] with resonator thickness comparable to the effective wavelength of incident light, or in multi-layer metallic structures [10, 17]. The excited electric and magnetic modes can be in phase in one direction and interfere constructively while they destructively interfere in the other direction. As a result, the radiation symmetry requirement is relaxed and giant transmission asymmetry for circular polarized lights can be realized, without requiring absorption on the metasurfaces. Besides utilising higher order resonance modes, building effectively bianisotropic metasurfaces is another common practice to acquire comprehensive control over electromagnetic waves including achieving high asymmetric transmission [17, 30, 31]. However, our metasurface is not bianisotropic and no magneto-electric coupling terms exist in the constitutive equations of electric and magnetic fields, due to the presence of inversion symmetry in the resonator [32–34].

3. Polarization robust geometric phase metasurfaces

In this section, we move our focus to the manipulation of the geometric phase of the transmitted circularly polarized light. The geometric phase (also known as Pancharatnam-Berry phase) manipulation is a robust method to impart abrupt phase shift locally on a metasurface; the phase change is not resonance-based and solely related to the geometrical orientation of the element, therefore the metasurface is easier to design [35, 36]. However, when compared to other phase manipulation approaches in metasurfaces including the propagation phase [37] and resonance phase shift [38], it has the disadvantage that it only works in circular polarization states, and only the transmitted light with polarization orthogonal to the incidence can acquire the geometric phase. On the Poincare sphere, it corresponds to a polarization state travelling from one pole to the other. For the co-polarized component there is no phase shift imparted [39] and it will bring noise to the target light of the correct CP. To this end, in the experimental setup, the combination of a linear polarizer followed by a quarter waveplate (QWP) is needed to filter one circular polarization for incidence and another set of QWP and linear polarizer is put after the sample to filter light of the desired handedness [26, 40]. These multiple optical elements are bulky and do not render themselves available to integrated nanophotonic system. To the best of our knowledge, so far, almost all geometric phase metasurfaces are done with achiral optical element, such as metal bars, complementary sieves, or v-shape nanoantenna, showing no difference in their response to RCP and LCP lights, except for the Z-shape apertures [41] which nevertheless didn't exhibit strong planar chirality. Very recently, there is a work published on spin-selective gradient chiral metasurface with geometric phase [42], however, it is a metallic metasurface functioning in the reflection mode and thus intrinsically different from our design.

As shown in the first part of this article, the planar chiral metasurface we proposed has the functionality of filtering light with desired handedness, and the transmitted light is converted into the opposite handedness with high efficiency. These special properties make it an ideal platform for a geometric phase metasurface without the need of those linear polarizers and QWPs. As linear polarization is a superposition of RCP and LCP, when a LP light with *any* azimuthal polarization angle is incident onto the metasurface, ideally, only half of the energy with the desired handedness can pass through while the other half is reflected. Based on the working principle of geometric phase metasurfaces, a phase shift of 2α will be imposed on the transmitted cross-polarized light when the Z-shape resonator is rotated locally by an angle α, giving the
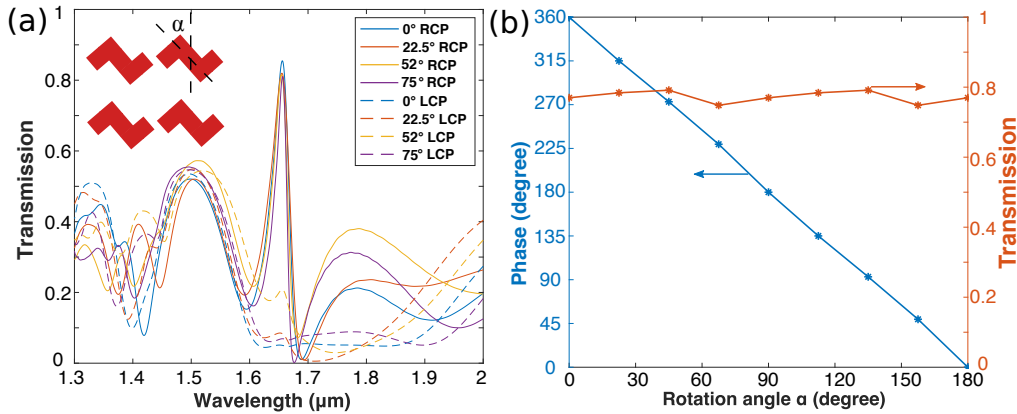
Fig. 5. (a) Transmission spectra for Z-shaped chiral resonator array with different orientation angle α under RCP (solid lines) and LCP (dashed lines) incidences. (b) The transmittance and phase of T_{LR} under different rotation angles at 1655 nm, showing transmittance constantly larger than 0.7 and the nearly linear phase range covering from 0 to 360 degrees.

phase-tuned transmission matrix:

$$\begin{pmatrix} E_{tl} \\ E_{tr} \end{pmatrix} = \frac{1}{2} \begin{pmatrix} t_{ll} & e^{-i2\alpha} t_{lr} \\ e^{i2\alpha} t_{rl} & t_{rr} \end{pmatrix} \begin{pmatrix} E_{0l} \\ E_{0r} \end{pmatrix} \qquad (3)$$

where E_0 and E_t denote the E-field of the incident and transmitted waves. With the two-fold rotational (C2) symmetry, the element is invariant after rotation of π around z-axis, so a continuous phase tuning range from 0 to 2π can be acquired.

However, it should be noted that the sharp transmission peak experiences a shift in the resonance frequency in response to the lattice environment change which affects the coupling among the resonators. In order to compensate for this effect and maintain the high transmission and the designated phase, the geometrical parameters of the resonators are slightly fine-tuned for each meta-atom. In the simulations for geometry optimization, each metasurface consists of only one kind of chiral meta-atom with the same rotated angle, with no difference in the geometries between neighboring unit cells. As the lattice resumes its original state after 90 degrees rotation, we only need to fine-tune the geometry and orientation angles for the four units with 0°, 45°, 90°, and 135° geometric phases, and the geometries and rotation angles for 180°, 225°, 270°, and 315° take the same values as for the first four angles. The initial simulation target is to let the transmission peaks overlap so that a high transmission rate can be maintained at the resonance wavelength, and then more elaborate adjustments were done to achieve the desired phases and amplitudes. The transmission spectra for those four modified units are plotted in Fig. 5(a), which shows that under RCP incidence the transmission peaks for meta-atoms with different geometric phases centred well at 1655 nm, while for LCP incidence, the transmission rate remains low for every meta-atom. The specific geometry parameters are listed in Table 1, from which we can see that the W1 and W2 parameters are slightly deviated from the original values, and extra rotation were applied for the 90° and 135° geometric phases. The amplitude and phase for the transmitted waves of the modified units are plotted in Fig. 5(b), at 1655 nm, showing that a constant transmission amplitude larger than 0.7 can be maintained with nearly linear geometric phase variation covering the whole 360 degrees range depending on the rotation angle of the meta-atom. With the capabilities of spontaneously filtering the desired circular polarization and

Table 1. The geometry parameters of the eight chiral meta-atoms for different geometric phases.

Meta-atom	1	2	3	4	5	6	7	8
Geometric phase	0°	45°	90°	135°	180°	225°	270°	315°
W1	200	205	220	215	200	205	220	215
W2	410	410	400	400	410	410	400	400
α	0°	22.5°	52°	75°	90°	112.5°	142°	165°
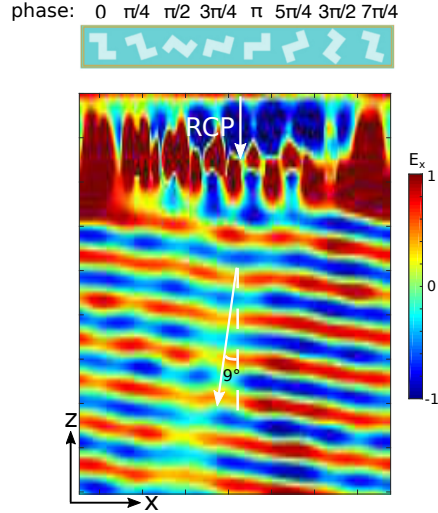
Fig. 6. Top: schematic of a supercell consisting of eight Z-shape resonators that provide a gradient phase increase from 0 to $\frac{7}{4}\pi$. Bottom: Ex fields of the anomalously refracted waves with RCP plane wave normal incidence at 1655 nm.

imposing a geometric phase into it, effectively, the metasurface combines the functionalities of a linear polarizer, a QWP, a spatial light modulator, a QWP, and a linear polarizer in sequence into one single device.

Firstly, we demonstrate the capability of the metasurface by anomalous transmission. We arrange the Z-shape resonators with different orientations from 0 to $\frac{7}{8}\pi$, which corresponds to geometric phases with $\frac{\pi}{4}$ linear phase gradient from 0 to $\frac{7}{4}\pi$, as shown on the top of Fig. 6. In principle, each unit is a Huygens' source with the assigned phase, and the superposition of the spherical waves from each source forms a plane wave of which the direction θ is determined by $sin(\theta) = \lambda/(n \cdot P)$, where $n = 1.45$ is the refractive index of the substrate and $P = 7.2\ \mu$m is the periodicity of the supercell consisting of eight units. In Fig. 6, the instantaneous real part of the transmitted Ex field is plotted for the RCP incidence at λ =1655 nm, which provides information on both the phase and amplitude. As shown in the figure, the wavefront of the transmitted wave is refracted 9 degrees to the surface normal, which agrees with the theoretical value, without the need of deliberately filtering out the co-polarized RCP components as in most geometric phase based metasurfaces, and it has a high transmission rate T = 0.7. The imperfection in the wavefront is caused by the coupling between neighbouring resonators and the interference from the small amount of unmodulated RCP component.

To further corroborate the function of the metasurface, we pattern the resonators to achieve a 2D hologram, which is an image created by the coherent interference of different point sources on the metasurface. Computer-generated holography (CGH) is a method to artificially design the
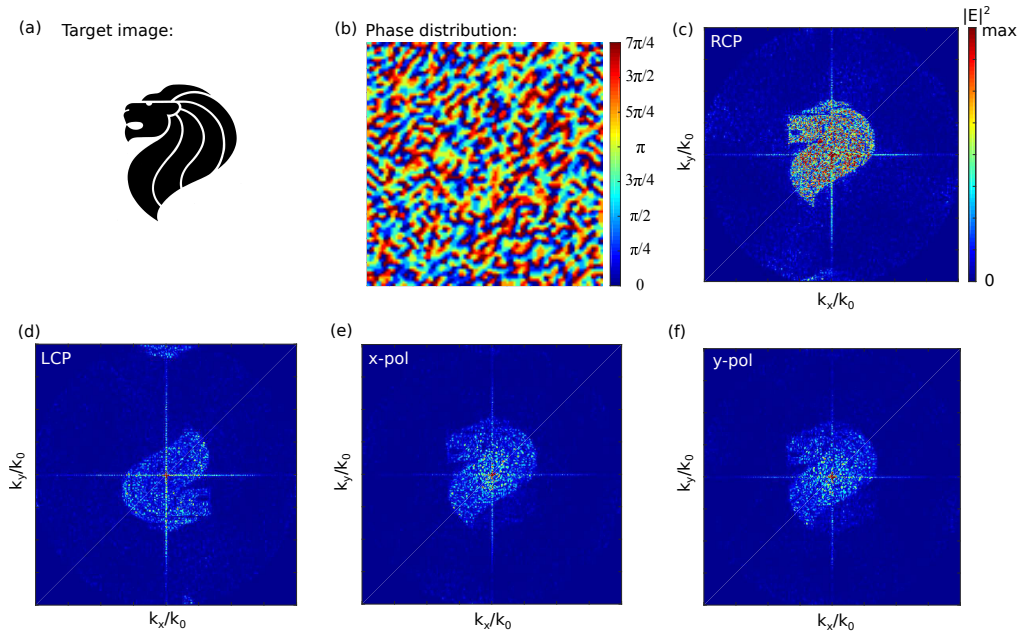
Fig. 7. (a) The target image for the 2D hologram. (b) Phase distribution of the metasurface with 100×100 unit pixels. (c) The generated hologram under RCP incidence at 1655 nm, showing a bright lion head logo. (d) The hologram under LCP incidence, showing a reversed logo, with greatly reduced amplitude. The holograms under (e) x-polarization and (f) y-polarization.

interference pattern that can generate holograms for non-existent objects. As shown in Fig. 7(a), a lion head logo was chosen as the target image. Considering the limited calculation capacity of a normal server, the image is sampled by 100×100 pixels. With eight phase levels and constant amplitude, the phase distribution pattern to generate the target image in the Fraunhofer region is calculated by the adaptive Gerchberg-Saxton phase-retrieval algorithm [43], with the retrieved phase distribution shown in Fig. 7(b). In the simulations, a plane monitor is placed one wavelength away from the resonator plane to record down the electric field vectors, then the far-field diffraction pattern is calculated through the vectorial angular spectrum theory [44]. Under RCP incidence, the generated image at $\lambda = 1655$ nm is plotted in Fig. 7(c), showing a clear logo with discernible details, and it has a high transmission rate of 0.7. The bright cross in the center of the image is a result of the rectangle aperture of the metasurface. In the figure, the x and y-axis of the hologram images are the normalised angular wavevectors k_x/k_0 and k_y/k_0 in x and y directions and k_0 is the wavevector in free space. Outside the circle of $k_x^2 + k_y^2 = k_0^2$, the fields are evanescent and do not propagate into the far-field. In geometric phase metasurfaces, as shown in Eq. 3, with the orthogonal circular polarization incidence, an opposite geometric phase is imparted [26]. As previously shown in Fig. 2(d), T_{RL} is non-zero at 1655 nm, there is still low transmission for LCP, with the opposite geometric phase. Therefore, under LCP incidence, the generated hologram is rotated 180 degrees around the origin, but the overall intensity is much weaker than that of the RCP, with transmission T = 0.2, so the hologram is dim as shown in Fig. 7(d). And under either x or y linear polarization incidence, the generated hologram is a coherent superposition of the holograms under RCP and LCP incidences. As the transmittance under RCP is much stronger than LCP, a straight hologram is generated as shown in Fig. 7(e) and 7(f), with the undesired ghost image from the other circular component overwhelmed by the right CP. The overall intensity is smaller than in Fig. 7(c) because only about half of the energy is transmitted.

With sufficiently large sample area and pixel numbers, the resolution of the hologram image can be further improved. Through this, we demonstrated a geometric phase-based holography metasurface that can function under any linear polarization state or elliptical polarization with the right handedness.

4. Conclusion

In summary, we proposed an all-dielectric planar chiral metasurface that exhibits near unity circular dichroism and asymmetric transmission for circularly polarized lights. The giant 2D chirality of 88% in such germanium metasurface greatly surmounts the fundamental limit of 25% in previous ultra-thin metallic metasurfaces, through the excitation of magnetic responses and the deliberate matching of the complex transmission coefficients of the co- and cross-polarized lights. Furthermore, the transmitted light from one particular handedness is efficiently converted to the opposite handedness, acquiring a geometric phase relying on the rotation angle. For any linear polarization state, one CP component is efficiently transmitted with an assigned geometric phase while the other circular component is reflected. Featured with these extraordinary properties, the chiral metasurface integrates the functions of cascaded linear polarizer, QWP, spatial light modulator, QWP, and linear polarizer, greatly reducing the number of required components in the optical path for geometric phase metasurfaces. The capabilities of the metasurface are demonstrated with anomalous transmission and a two-dimensional hologram under different polarization states. Our proposed idea and method pave the way for ultra-compact integrated metasurface devices with high efficiency.